

An integrated model of scattering from an imperfect interface

John G. Harris
Theoretical and Applied Mechanics, UIUC
216 Talbot Laboratory, 104 South Wright Street
Urbana, IL 61801

Douglas A. Rebinsky
Mechanical and Aerospace Engineering
Rutgers University
Piscataway, NJ 08854

Gerry Wickham
Department of Mathematics
University of Manchester
Manchester, M13 9PL

Abstract

We consider the anti-plane shear, SH or scalar problem of scattering from an interface characterized by a narrow region of heterogeneity. An approximate integral representation of the scattered wave fields in terms of a Green's function for a reference problem, and the stress and momentum polarizations averaged through the thickness of the interface is derived. Providing certain material contrast parameters are $O(1)$, the error in this expression is formally $O(kh)^2$, where k is the wave number and $2h$ is the thickness of the interface. To find the unknown polarizations we specialize to a model configuration that is periodic over a length scale much greater than the characteristic length scales of the inhomogeneities in the interface. This allows an exact formulation in terms of an infinite system of algebraic equations. Expressions modeling the reflection and transmission measured by a coaxial, confocal pair of transducers are then derived so that the effects of the transducer can be included in the modeling. These coefficients are calculated in terms of the solution of the algebraic system. We present numerical results for several different model interfaces.

PACS numbers: 43.20.Gp, 43.20.Rz, 43.35.Zc

INTRODUCTION

Interfaces formed by the faces of fatigue cracks and along diffusion bonds exhibit roughness and partial contact at many length scales. Those features whose sizes are on the order of a wavelength or greater produce distinguishable scattered signals, whereas smaller features contribute to background scattering that might be considered as noise. Our goals in this paper are firstly to construct a general model of an imperfect interface exhibiting this level of complexity, secondly to describe the scattering of an acoustic wave from such an interface and thirdly to relate the scattered wave fields to measured reflection and transmission coefficients. Our approach combines the polarization integral equations derived by Wickham¹ to describe scattering from a thin interface and the measurement model used by Yogeswaren and Harris² to describe reflection and transmission at an interface consisting of several coplanar cracks. We consider the anti-plane shear or SH problem. Although this undoubtedly limits the applicability of the work, we anticipate that it captures many of the important qualitative physical features of the three dimensional problem.

The study that served to motivate the present calculation is that of Margetan et al³. They interrogated model interfaces with compressional waves, and have reported experimental results for generalized transmission and reflection coefficients. They define each coefficient (Eq.(6) of Ref.3) as the Fourier component, at a given frequency, of the signal transmitted by or reflected from the interface divided by the temporal Fourier component of a reference signal at the same frequency. Signals resulting from reflection from the transducer followed by subsequent reflection or transmission by the interface are not used in this measurement. Although imperfections occur at many length scales they were concerned with those whose lengths are on the order of a compressional wavelength in a metal (typically aluminium) using frequencies on the order of 5 to 10 MHz. Focused transducers arranged as a coaxial confocal pair were used to direct ultrasound across a thin fluid couplant interface and into a solid, with approximate focusing taking place at the interface. The transducers had apertures 1 to 1.5 cm in radius and were designed to focus in water at approximately 9 cm from the face of the transducer. During an inspection of an interface the transducers were scanned quasi-statically through from two hundred to four hundred steps where each step is 0.06 mm. Because the transducer apertures are several wavelengths in radius, at each position, the signals scattered from several inhomogeneities in the interface along with signals resulting from multiple scattering among the

inhomogeneities are collected. Each transducer's voltage is the summed magnitude and phase of all these signals.

Several recent papers concerned with modeling interfaces and their scattered signals are of direct interest here. A. Bostrom⁴ used an integral equation approach to calculate the scattering from cracks having a boundary condition comprised of equivalent springs that modeled partial contact. Moreover he used a reciprocity relation to model aspects of the probe's response to the scattered signals. Pecorai et al⁵ extend a quasi-static boundary condition for contact at an imperfect interface to randomly irregular interface profiles. They then consider scattering from this model interface, using a perturbation technique where the ratio of the roughness height to wavelength is the small parameter. They also assume the profile has a small slope. Qu⁶ takes a different approach and models the interface as an array of cracks from which anti-plane shear waves are scattered. The cracks are randomly distributed along an interface between contrasting materials and multiple scattering is approximately accounted for. Achenbach et al⁷ summarize their work on various interface models all of which are comprised of a layer of compact inhomogeneities. Scattering from both cracks and cavities in two and three dimensions is calculated, though a certain emphasis is given to periodically distributed inhomogeneities. Shiloh, et al⁸ considered scalar, two dimensional models of scattering from complex interfaces using the analogy of focused ultrasonic systems with their optical counterparts. They placed less emphasis upon the multiple interaction aspect of the scattering, and emphasized the noise that small scatterers introduce into the detection of larger objects.

It is very difficult to launch a focused wave into a solid, though Thompson, et al.⁴ report some success in having done so. They succeed in focusing at a plane in aluminium approximately 20 compressional wavelengths, at 10 MHz, below the surface and in achieving a focal region on the order of 2 compressional wavelengths in diameter. In principle, defects on the order of 2 mm could be resolved, though the refraction at the solid interface as the sound enters the solid causes the focal region to be quite aberrated and its exact size hard to determine. Here we also consider interrogating the interface with a focused beam. We consider detecting both individual defects and clusters of defects with limited resolution among them, though we do not view the smaller defects as causing background noise. Rather we attempt to take some account of their collective scattering behavior. This was also done in the numerical examples of Ref. 2 where only larger well separated defects were resolved.

As indicated previously the results are presented as generalized transmission and reflection coefficients. By considering anti-plane shear scattering from an array of cracks, Yogeswaren and Harris² suggested definitions of generalized transmission and reflection coefficients that, apart from their normalization, approximate those measured by Margetan et al.³. Their central hypothesis was that these coefficients are a consequence of an integration of all the scattered waves striking the aperture, but that among those waves the dominant contributions come from those that phase match to the incident wave. We adopt that same hypothesis here and develop its consequences using the more general model of the interface constructed by Wickham¹. We present numerical results for several model interfaces constructed from arrays of cylinders and one constructed from grazing sinusoids.

I POLARIZATION THEORY

A. Formulation

INSERT FIGURE 1

Our purpose is to examine the reflection from and transmission through a general interface insonified by a focused beam. Thus we anticipate a localized interaction over a region small compared with some characteristic length scale a along the interface (the x_1 direction). A mathematically convenient way to model this situation is to imagine that the finite interface being insonified can be extended to infinity in both directions by embedding it in a relatively large cell of width $2a$, and then periodically continuing the cell and imposing periodic boundary conditions at the cell boundaries. Within each cell scatterers at many smaller variations in characteristic size are enclosed. These scatterers may also have different mechanical properties and may model the presence of inclusions, voids or a locally varying state of pre-stress. Further, or alternatively, the geometry of the interface may vary so as to model the degree of contact between mating surfaces. Figure 1 shows one such situation. Here two partially contacting surfaces indicate a fatigue crack that is growing from the tip of a fully developed one. Our calculations are intended to model interrogating this end zone. Provided the interrogating beam is kept well within the cell, the presence of the fully developed crack at one side should not radically affect the transmitted and reflected signals. Moreover, it is reasonable to assume that the scattered wave field within the cell will be overwhelmingly that caused by the interface within that cell and not be greatly affected by periodic extensions of the interface. The strategy of

introducing the periodicity may be regarded as a mathematical device that effectively truncates the domain of integration of the partial differential equations to an infinite strip of finite width.

We consider an interface, as shown in Fig.1, consisting of a thin heterogeneous layer V_0 , whose global thickness is $2h$, separating two half space regions V^\pm filled with the same homogenous isotropic material. The regions are bounded at $x_1 = \pm a$. We assume that the motion in the composite body is time harmonic with frequency ω and is two-dimensional relative to Cartesian coordinates $(x, y, z) \equiv (x_1, x_2, x_3)$ fixed at the interface. Further, we assume that the only nonzero component of the total displacement \mathbf{u} is the x_3 component. The equation of motion in V^\pm is

$$\partial_\beta \tau_{\beta 3} + \rho \omega^2 u_3 = 0 \quad \mathbf{x} \in V^+ \cup V^- \quad (1)$$

where the subscript β takes the values 1 and 2, and \mathbf{x} is a vector in (x_1, x_2) . The constitutive relation is simply

$$\tau_{\beta 3} = \mu \partial_\beta u_3 \quad (2)$$

In the heterogeneous region, characterized by $\mu^*(\mathbf{x})$ and $\rho^*(\mathbf{x})$, we define stress and momentum polarizations as

$$\sigma_{\beta 3} = (\mu^* - \mu) \partial_\beta u_3 \quad \text{and} \quad p_3 = \omega(\rho^* - \rho) u_3 \quad (3a,b)$$

respectively. It then follows that the field equation in the layer may be written as

$$\partial_\beta \tau_{\beta 3} + \rho \omega^2 u_3 = -\partial_\beta \sigma_{\beta 3} - \omega p_3 \quad \mathbf{x} \in V_0 \quad (4)$$

The assumption of global periodicity implies that the preceding differential equations need only be solved within a single cell subject to the periodic boundary conditions

$$u_3(-a, x_2) = u_3(a, x_2) \quad \text{and} \quad \tau_{13}(-a, x_2) = \tau_{13}(a, x_2) \quad (5a,b)$$

Let the incident wave field be denoted by u_3^i , so that

$$u_3 = u_3^i + u_3^s \quad \mathbf{x} \in V^+ \cup V^- \quad (6)$$

where u_3^s is the scattered wave field in each cell. We take both the incident and scattered wave fields separately to satisfy Eq.(5). The scattered wave field consists of only outgoing waves as $|x_2| \rightarrow \infty$. Finally, to complete the formulation we need to specify conditions at the boundary S between $V^+ \cup V^-$ and V_0 . Here we assume that the two materials are perfectly bonded so that the net traction and displacement are continuous across S .

B. Derivation of the polarization integral equations

The appropriate Green's function $u_3^g(\mathbf{x}, \mathbf{y})$, for our derivation, is that for the periodic cell without an interface. It satisfies

$$\partial_\beta \tau_{\beta 3}^g + \rho \omega^2 u_3^g = -\mu \delta(\mathbf{x} - \mathbf{y}) \quad , \quad -a < x_1 < a \quad (7)$$

subject to the periodic boundary conditions

$$u_3^g(-a, x_2, y) = u_3^g(a, x_2, y) \quad \text{and} \quad \tau_{13}^g(-a, x_2, y) = \tau_{13}^g(a, x_2, y) \quad (8)$$

The Green's stress $\tau_{\beta 3}^g$ is related to the Green's displacement by Eq.(2). The Green's function is

$$u_3^g(\mathbf{x}, \mathbf{y}) = \frac{i}{4ka} \sum_{n=-\infty}^{\infty} \frac{1}{\kappa_n} e^{ik[(n\pi/ka)(x_1-y_1) + \kappa_n|x_2-y_2|]} \quad (9)$$

where k is the wave number,

$$\kappa_n = [1 - (n\pi/ka)^2]^{1/2} \quad (10)$$

and the branch cuts are defined by asking that $\text{Im}(\kappa_n) \geq 0 \forall n$. Note that, by using the Poisson sum formula¹¹, u_3^g can be expressed as a sum of Hankel functions and that, provided ka is large, the Hankel function for the cell between $x_1 = \pm a$ will be dominant.

We now apply the reciprocity theorem in $V^+ \cup V^-$ to the outwardly radiating wave fields u_3^s and u_3^g . This gives

$$[1 - \chi(V_0)]u_3^s(y) = -\frac{1}{\mu} \int_{S^+} [\tau_{\beta 3}^s(\mathbf{x})u_3^g(\mathbf{x}, y) - \tau_{\beta 3}^g(\mathbf{x}, y)u_3^s(\mathbf{x})] n_\beta dS(\mathbf{x}) \quad (11)$$

where n_β is the outward normal to V_0 and S^+ is S approached from outside V_0 . The indicator $\chi(V_0)$ is defined as

$$\chi(V_0) = \begin{cases} 1 & \mathbf{y} \in V_0 \\ 0 & \mathbf{y} \notin V_0 \end{cases} \quad (12)$$

The periodic boundary conditions satisfied by the reciprocating wave fields ensure that there is no contribution from the surfaces $x_1 = \pm a$. Next we apply the reciprocity theorem to V_0 where $u_3^s = u_3$ throughout the interior of V_0 . This gives

$$\begin{aligned} \chi(V_0)u_3(y) &= \frac{1}{\mu} \int_{V_0} [\partial_\beta \sigma_{\beta 3}(\mathbf{x}) + \omega p_3(\mathbf{x})] u_3^g(\mathbf{x}, y) dV(\mathbf{x}) \\ &\quad + \frac{1}{\mu} \int_{S^-} [\tau_{\beta 3}(\mathbf{x})u_3^g(\mathbf{x}, y) - \tau_{\beta 3}^g(\mathbf{x}, y)u_3(\mathbf{x})] n_\beta dS(\mathbf{x}) \end{aligned} \quad (13)$$

where S^- is S approached from inside V_0 . Adding Eqs.(11) and (13) we obtain

$$\begin{aligned} u_3^s(y) &= \frac{1}{\mu} \int_{V_0} [\partial_\beta \sigma_{\beta 3}(\mathbf{x}) + \omega p_3(\mathbf{x})] u_3^g(\mathbf{x}, y) dV(\mathbf{x}) \\ &\quad - \frac{1}{\mu} \int_S \{ [\tau_{\beta 3}^s(\mathbf{x})] u_3^g(\mathbf{x}, y) - \tau_{\beta 3}^g(\mathbf{x}, y) [u_3^s(\mathbf{x})] \} n_\beta dS(\mathbf{x}) \end{aligned} \quad (14)$$

for $\mathbf{y} \in V_0 \cup V^+ \cup V^-$. The terms [...] in the integrand of the second integral denote jumps across S . Using the condition of perfect bonding it is seen that

$$\begin{aligned} &\int_S \{ [\tau_{\beta 3}^s(\mathbf{x})] u_3^g(\mathbf{x}, y) - \tau_{\beta 3}^g(\mathbf{x}, y) [u_3^s(\mathbf{x})] \} n_\beta dS(\mathbf{x}) \\ &= \int_{S^-} \sigma_{\beta 3}(\mathbf{x}) u_3^g(\mathbf{x}, y) n_\beta dS(\mathbf{x}) - \int_{S^+} [\tau_{\beta 3}^i(\mathbf{x}) u_3^g(\mathbf{x}, y) - \tau_{\beta 3}^g(\mathbf{x}, y) u_3^i(\mathbf{x})] n_\beta dS(\mathbf{x}) \end{aligned} \quad (15)$$

Finally, assuming that the incident wave field has an analytic continuation into the interior of V_0 , a third application of the reciprocity theorem yields

$$\chi(V_0)u_3^i(y) = \frac{1}{\mu} \int_S [\tau_{\beta 3}^i(\mathbf{x})u_3^g(\mathbf{x}, y) - \tau_{\beta 3}^g(\mathbf{x}, y)u_3^i(\mathbf{x})] n_\beta dS(\mathbf{x}) \quad (16)$$

Performing an integration by parts in the first integral on the right hand side of Eq.(14) and combining the result with Eqs.(15) and (16) yields an integral representation for the total wave field, namely

$$u_3(y) = u_3^i(y) - \frac{1}{\mu} \int_{V_0} [\sigma_{\beta 3}(\mathbf{x}) \partial_\beta u_3^g(\mathbf{x}, y) - \omega u_3^g(\mathbf{x}, y) p_3(\mathbf{x})] dV(\mathbf{x}) \quad (17)$$

We have thus shown that the entire scattered wave field, including that internal to V_0 , is determined by the polarizations $\sigma_{\beta 3}$ and p_3 .

C. An approximate representation

Here we are concerned with interfaces where the dimensionless parameter $(kh) < 1$. This suggests that we approximate the Green's terms by their values on the mean plane $x_2 = 0$, corresponding to the first term in a Taylor series in powers of (kx_2) . We can then complete the x_2 integration in Eq.(17) by replacing the unknown polarizations by the through thickness means. Provided the material contrasts

$$M^* = (\mu^*/\mu - 1) \quad \text{and} \quad D^* = (\rho^*/\rho - 1) \quad (18a, b)$$

are not too great the average polarizations are $O(kh)$. However, even when the material contrasts are stronger our approximation should be useful because the polarizations themselves are not being approximated. Wickham^{1,11} discusses these issues further. We thus replace Eq.(17) by

$$u_3(y) = u_3^i(y) - \frac{h}{\mu} \int_{-a}^a [\hat{\sigma}_{\beta 3}(x_1) \partial_\beta u_3^g(x_1, y) - \omega u_3^g(x_1, y) \hat{p}_3(x_1)] dx_1 \quad (19)$$

where

$$\hat{\sigma}_{\beta 3} = \frac{1}{h} \int_{-h\eta^-}^{h\eta^+} \sigma_{\beta 3} dx_2 \quad \text{and} \quad \hat{p}_3 = \frac{1}{h} \int_{-h\eta^-}^{h\eta^+} p_3 dx_2 \quad (20a, b)$$

The upper and lower boundaries, controlling the degree of contact of the interface, are described by $x_2 = h\eta^\pm(x_1/a)$. Note that, in the Green's terms, x_2 has been set to zero and then suppressed in Eq.(19) and that the surface S now denotes the x_1 axis. For the interfaces of interest here, we assume that the error in Eq.(19) is at most $O(kh)^2$. From this representation a vector integral equation for the unknown mean polarizations maybe derived. However, in the next section, we proceed directly to a solution scheme in terms of an infinite system of algebraic equations.

D. An infinite system of algebraic equations

We shall assume that not only are ρ and μ constant in the surrounding reference material, but that ρ^* and μ^* in the interface are also constant. To further simplify the exposition, we take the x_1 axis to be a plane of reflection symmetry so that $\eta^+ = -\eta^-$. This is not an essential constraint and our approach can be applied to interfaces having no symmetry.

We start by introducing the finite Fourier transform of the unknown average polarizations in the form

$$\hat{\sigma}_{\beta 3} = \mu \sum_{q=-\infty}^{\infty} \xi_{\beta q} e^{iq\pi x_1/a} \quad \text{and} \quad -\hat{p}_3 = \rho c \sum_{q=-\infty}^{\infty} \xi_{3q} e^{iq\pi x_1/a} \quad (21a,b)$$

where the coefficients are

$$\xi_{\beta m} = \frac{1}{2\mu} \int_{-1}^1 \hat{\sigma}_{\beta 3} e^{-im\pi\gamma} d\gamma \quad \text{and} \quad \xi_{3m} = -\frac{1}{2\rho c} \int_{-1}^1 \hat{p}_3 e^{-im\pi\gamma} d\gamma \quad (22a,b)$$

and c is the wave speed of the host material. The scattered wave field is then given by

$$u_3(y) = u_3^i(y) - \frac{h}{2} \sum_{n=-\infty}^{\infty} \frac{1}{\kappa_n} [\xi_n + \kappa_n \operatorname{sgn}(y_2) \xi_{2n}] e^{ik[(n\pi/ka)y_1 + \kappa_n|y_2|]} \quad (23)$$

where

$$\xi_n = (n\pi / ka)\xi_{1n} + i\xi_{3n} \quad (24)$$

and $\text{sgn}(x)$ denotes the distribution $[2H(x) - 1]$. Essentially we are expressing the wave field as a sum of the modes of the waveguide formed by each cell. An infinite system of algebraic equations for the unknown Fourier coefficients ξ_n and ξ_{2n} is constructed by forcing self-consistency on Eq.(23).

Consider the ξ_{2n} equation. Firstly calculate the mean polarization $\hat{\sigma}_{32}$ using Eqs.(20a) and (23). Note that differentiating the $\text{sgn}(x)$ gives $2\delta(x)$. Secondly use this expression in Eq.(22a) to give

$$\left(\frac{\mu^*}{\mu}\right) \xi_{2m} = b_{2m} + M^* \sum_{n=-\infty}^{\infty} a_{mn} \xi_{2n} \quad , \quad -\infty \leq m \leq \infty \quad (25)$$

where the a_{mn} and b_{2m} are defined following Eq.(27). Repeating these steps for $\hat{\sigma}_{31}$ and \hat{p}_3 gives

$$\xi_{1m} = b_{1m} + M^* \sum_{n=-\infty}^{\infty} \frac{n\pi}{\kappa_n^2 ka} a_{mn} \left[\left(\frac{n\pi}{ka}\right) \xi_{1n} + i\xi_{3n} \right] \quad , \quad -\infty \leq m \leq \infty \quad (26)$$

and

$$\xi_{3m} = b_{3m} + D^* \sum_{n=-\infty}^{\infty} \frac{i}{\kappa_n^2} a_{mn} \left[\left(\frac{n\pi}{ka}\right) \xi_{1n} + i\xi_{3n} \right] \quad , \quad -\infty \leq m \leq \infty \quad (27)$$

The a_{mn} are given by

$$a_{mn} = \delta_{mn} - \frac{1}{2} \int_{-1}^1 e^{ikh\kappa_n \eta(\gamma)} e^{-i(m-n)\pi\gamma} d\gamma \quad (28)$$

and the b_{jm} by

$$b_{\beta m} = \frac{1}{2\mu} \int_{-1}^1 \hat{\sigma}_{\beta 3}^i e^{-im\pi\gamma} d\gamma \quad \text{and} \quad b_{3m} = -\frac{1}{2\rho c} \int_{-1}^1 \hat{p}_3^i e^{-im\pi\gamma} d\gamma \quad (29a,b)$$

The $\hat{\sigma}_{\beta 3}^i$ and \hat{p}_3^i are the mean incident polarizations. Defining

$$b_n = (n\pi / ka)b_{1n} + ib_{3n} \quad (30)$$

and noting Eq.(24), Eqs.(26) and (27) may be combined to yield the single system

$$\xi_m = b_m + \sum_{n=-\infty}^{\infty} \frac{1}{\kappa_n^2} [M^* \left(\frac{n\pi}{ka}\right) \left(\frac{m\pi}{ka}\right) - D^*] a_{mn} \xi_n, \quad -\infty \leq m \leq \infty \quad (31)$$

The contrasts M^* and D^* are defined by Eq.(18). We are thus left with two uncoupled infinite systems of algebraic equations to solve. We obtain an approximate solution by truncating the system so that it only includes contributions from the propagating modes. That is n is limited to values such that κ_n is real. Physically, we are omitting any evanescent scattered waves because we do not anticipate that they will make a significant contribution to the signals detected by the transducers.

II A MEASUREMENT MODEL

We now introduce definitions of the generalized reflected and transmitted coefficients. The suggested definitions model the fact that a transducer integrates all the scattered waves striking its aperture to produce a voltage, but that, among those waves, the dominant contributions come from those that phase match to the incident wave.

A. An incident beam

A plane wave incident at an arbitrary angle to the interface shown in Fig.1 can be represented as

$$u_3 = e^{ik[(n\pi/ka)x_1 + \kappa_n x_2]} \quad (32)$$

where κ_n is given by Eq.(10). This suggests that we may construct a more general incident wave field as

$$u_3 = \sum_{n=-N}^N E(n\pi / ka) e^{\pm ik[(n\pi/ka)X_1 + \kappa_n |x_2|]} \quad (33)$$

where

$$X_1 = x_1 - s \quad (34)$$

The offset s is introduced so that we may later vary the position of the axis of the confocal arrangement. The plus sign indicates a wave outgoing from the interface, while the minus sign indicates one that is incoming. The term κ_n is defined as in Eq.(10) and N will be chosen so that all the κ_n are real. That is N will be set to the greatest integer less than ka/π . Physically, we are omitting any evanescent waves that the source may excite because we do not anticipate that they will make a significant contribution to the scattering at the interface. It remains to specify the coefficients $E(n\pi / ka)$ so that Eq.(33) will model a focused beam whose focal region is symmetrically centered about $(s,0)$. The geometry is indicated in Fig.2.

INSERT FIGURE 2

To motivate our selection of the $E(n\pi / ka)$ we note that the Poisson summation formula¹¹ implies that, at $x_2 = 0$,

$$\sum_{q=-\infty}^{\infty} \phi(X_1 - 2aq, 0) = \sum_{n=-\infty}^{\infty} E(n\pi / ka) e^{ik(n\pi / ka)X_1} \quad (35)$$

where

$$\phi(X_1, x_2) = \frac{ka}{\pi} \int_{-\infty}^{\infty} E(\xi) e^{\pm ik(\xi X_1 + \kappa(\xi)|x_2|)} d\xi \quad (36)$$

and $E(n\pi/ka) = 0$ for $n > N$. The function $\kappa(\xi)$ is defined as indicated in Eq.(10) with ξ replacing $(n\pi / ka)$. Next we imagine that the incoming wave field

$$\phi = Ae^{-(X_1/g)^{2b}} \frac{e^{-ikR}}{(kR)^{1/2}} \Big|_{x_2=-f} \quad (37)$$

fills the aperture of the source S_e at $x_2 = -f$. The distance

$$R(X_1, x_2) = (X_1^2 + x_2^2)^{1/2} \quad (38)$$

is that from $(s, 0)$ to a point in the aperture S_e (for the arguments shown). The parameters g and b are free and may be chosen to adjust the cross section of the beam. And A is a constant fixing the amplitude. Next we match Eq.(37) to the far field ($kR \gg 1$) asymptotic approximation of Eq.(36). Note that the dominant term, for $s < a$, is that coming only from the cell $q = 0$. The method of constructing the beam is close to that used in Rebinsky and Harris¹². This gives

$$E(n\pi / ka) = [U_3 / (2ka\kappa_n)] e^{-[n\pi F / (ka\kappa_n)]^{2b}} \quad (39)$$

INSERT FIGURE 3

where $F = f/g$ and $U_3 = [e^{-i\pi/4} (2\pi)^{1/2} A]$. The number F is similar to but not identical with the eff-number in optics. Equation (33) both satisfies the wave equation and the periodic boundary conditions, and has sufficient parameters that, by making satisfactory choices of these, it models a focused beam.

It may appear that we must arrange that $g/a < 1$. However, this is not the case and is indicated by the fact that only the ratio F appears in our model of the beam. As long as the incident sound, at the interface, is largely confined within the $q = 0$ or $[-a, a]$ cell, then our construction of the incident beam ensures that we are always dealing with the scattering induced within $[-a, a]$.

With the focused beam as our incident wave field, $\hat{\sigma}_{32}^i$ is

$$\frac{\hat{\sigma}_{32}^i}{\mu} = \frac{1}{h} M^* \sum_{n=-N}^N E(n\pi / ka) F_2(X_1, \eta) \quad (40)$$

where

$$F_2(X_1, \eta) = e^{ik(n\pi/ka)X_1} (e^{ikh\kappa_n\eta} - 1) - e^{-ik(n\pi/ka)X_1} (e^{-ikh\kappa_n\eta} - 1) \quad (41)$$

The other two polarizations are given by similar expressions. From these and Eq.(29a) the b_{jm} are given by the following.

$$b_{1m} = -\frac{1}{h} M^* \sum_{n=-N}^N \frac{1}{\kappa_n} \left(\frac{n\pi}{ka} \right) E(n\pi / ka) (e^{-iks(n\pi/ka)} a_{mn} + e^{iks(n\pi/ka)} a_{(-m)n}^*) \quad (42)$$

$$b_{2m} = -\frac{1}{h} M^* \sum_{n=-N}^N E(n\pi / ka) (e^{-iks(n\pi/ka)} a_{mn} - e^{iks(n\pi/ka)} a_{(-m)n}^*) \quad (43)$$

and

$$b_{3m} = -\frac{i}{h} D^* \sum_{n=-N}^N \frac{1}{\kappa_n} E(n\pi / ka) (e^{-iks(n\pi/ka)} a_{mn} - e^{iks(n\pi/ka)} a_{(-m)n}^*) \quad (44)$$

The a_{mn} are given by Eq.(28). Note at this point that we have characterized the scattering problem by three sets of important coefficients, the E_n describing the incident wave field, the a_{mn} , defined by Eq. (28), describing the geometry of the interface, and the material contrasts M^* and D^* , defined by Eq.(18).

B. Transmission and reflection coefficients

Consider the configuration shown in Fig.2. We show two transducers whose apertures are represented by the surfaces S_r and S_e . Though the scattering model and therefore the imagined transducers are two-dimensional, we want our modeling to capture the essential physical feature that the many signals scattered from the interface are collected by the transducers and that these signals are added in magnitude and phase to produce a single measured quantity. At S_r a transmission coefficient is measured, while at S_e a reflection coefficient is measured. Here we define these coefficients in such a way that they are sums of all the received signals and then we relate these coefficients to the scattered wave field at the interface.

Following the work of Section IB we can use the reciprocity theorem to relate the responses at S_r and S_e to that at the interface. Suppose that $(u_3^1, \tau_{3\beta}^1)$ and $(u_3^2, \tau_{3\beta}^2)$ are two anti-plane shear wave fields satisfying the periodicity relations, Eq.(8). Further, suppose that the first wave field is an arbitrary superposition of plane waves and the second is the solution to the present problem. That is, u_3^2 denotes the incident beam, Eq.(33), plus the corresponding wave field scattered from the interface. Then we find that

$$\int_{S_r} - \int_{S_e} (u_3^1 \tau_{32}^2 - u_3^2 \tau_{32}^1) dx_1 = h \int_{-a}^a (\hat{\sigma}_{3\beta}^2 \partial_\beta u_3^1 - \omega u_3^1 \hat{p}_3^2) dx_1 \quad (45)$$

Following the work of Section IC we have approximated the wave field $(u_3^1, \tau_{3\beta}^1)$ by its values on the mean plane $x_2 = 0$ and again the average polarizations are given by Eqs.(20a, b). As mentioned previously, g/a need not be less than 1. If S_r and S_e spill into an adjacent cell, then the global periodicity of the problem enables us to pick a new cell that completely includes S_r and S_e . The periodic boundary conditions will also hold along the boundaries of this new cell. Further we have constructed the incident beam such that S_e emits the sound inducing the mean polarizations in the $[-a, a]$ cell given in the right integration of Eq.(45). Lastly, note that Eq.(45) neglects energy that does not fall on the apertures themselves. We anticipate that in the confocal arrangement considered here this is a reasonable approximation.

To calculate the transmission coefficient measured at S_r we take $(u_3^1, \tau_{3\beta}^1)$ to be a disturbance equal to the complex conjugate of Eq.(33), with $E(n\pi/ka)$ given by Eq.(39). Wave field 1 then represents a focused beam, its focal plane being the interface, propagating from S_r to S_e . This selection ensures that the first term on the left hand side of Eq.(45) provides an integrated measure of the response over the aperture S_r to the wave fields scattered from within $[-a, a]$. To evaluate the integrals on the left hand side of Eq.(45) we need approximate expressions for $(u_3^1, \tau_{3\beta}^1)$ and $(u_3^2, \tau_{3\beta}^2)$ at S_r and S_e . We consider transmission. Reversing the argument used to motivate the construction of the incident beam, we can approximate u_3^1 as

$$u_3^1(\mathbf{x}) = \frac{ka}{\pi} \left(\frac{2\pi}{kR} \right)^{1/2} E^*(X_1/R) \frac{|x_2|}{R} e^{\pm i\pi/4} e^{\mp i k R} \quad (46)$$

where the plus sign is taken when $x_2 < 0$ and the minus sign when $x_2 > 0$. The distances X_1 and R are defined by Eqs.(34) and (38), respectively.

Finding an expression for the scattered wave fields at the apertures is not so straightforward. The principal steps are as follows. Firstly, express the Green's function, Eq.(9), as a sum of Hankel functions using the Poisson sum formula. Secondly, substitute this representation into Eq.(19). We are concerned only with the response measured at S_r and S_e so that only the Hankel function describing the scattered wave field excited in the principal cell $[-a, +a]$ needs to be retained. By doing so we are ensuring that we are

mapping the scattered wave field back to the surfaces S_r and S_e , even when parts of these surfaces parts may lie in an adjacent cell. Lastly, the remaining Hankel function is approximated by its far field form. The asymptotic wave field, transmitted by the interface within the cell $[-a, a]$, can be then written as

$$u_3^2(\mathbf{x}) = T_r(\mathbf{x}) \frac{ka}{\pi} \left(\frac{2\pi}{kR}\right)^{1/2} E(X_1/R) \frac{|x_2|}{R} e^{-i\pi/4} e^{ikR} \quad (47)$$

where $T_r(\mathbf{x})$ is

$$T_r(\mathbf{x}) - 1 = \frac{ih}{4E(X_1/R) |x_2|/R} \times \int_{-1}^1 e^{ik\phi(X_1, x_2; s-av)} \left(\frac{R(X_1, x_2)}{R(X_1 + s - av, x_2)} \right)^{1/2} \left[\frac{\hat{\sigma}_{31}(av)}{\mu} \sin \theta + \frac{\hat{\sigma}_{32}(av)}{\mu} \cos \theta - i \frac{\hat{p}_3(av)}{\rho c} \right] dv \quad (48)$$

and

$$\phi(X_1, x_2; s - av) = R(X_1 + s - av, x_2) - R(X_1, x_2) \quad (49)$$

The angle θ is defined by

$$\tan \theta = \frac{X_1 + s - av}{|x_2|} \quad (50)$$

and X_1 and R are defined by Eqs.(34) and (38), respectively. Unless the argument is explicitly shown $R = R(X_1, x_2)$. Note that $T_r(\mathbf{x})$ is a pointwise transmission coefficient depending upon the point of observation and that it is a consequence of all the scattering taking place at the interface.

To analyze $T_r(\mathbf{x})$ further, write it as

$$T_r(\mathbf{x}) - 1 = \int_{-1}^1 [1 - \gamma(v)] M(\mathbf{x}, v) e^{ik\phi} dv + \int_{-1}^1 \gamma(v) M(\mathbf{x}, v) e^{ik\phi} dv \quad (51)$$

where the slowly varying part of the integrand is symbolized by $M(\mathbf{x}, v)$ and $\gamma(v)$ is a neutralizer¹³ defined such that

$$\gamma(v) \rightarrow 0 \quad \text{as} \quad v \rightarrow s/a \pm \varepsilon, \quad \varepsilon > 0; \quad \text{and} \quad \gamma(s/a) = 1 \quad (52)$$

The ε can be taken to be very small. The first integral in Eq.(51) is of order¹³ $(kd_a)^{-1}$ where d_a is the distance from an end point $\pm a$ to the point of observation. Thus, to the order of approximation considered here, this term may be ignored. The integrand of the second integral can be approximated using

$$\exp(ik\phi) = 1 - a_1(\mathbf{x})(v - s/a) + O(v - s/a)^2 \quad (53)$$

where the Taylor coefficient $a_1(\mathbf{x})$ depends upon the point of observation, but not on v . Accordingly, the principal contribution to $T_r(\mathbf{x})$ comes from scattering in the neighborhood of $x_1 = s$, precisely the response that we should expect from a focused incident beam. To the same degree of approximation $\partial T_r / \partial x_2$ is zero (though T_r depends upon \mathbf{x}) and we find that

$$\tau_{32}^2 = \mu \frac{k^2 a}{\pi} \left(\frac{2\pi}{kR} \right)^{1/2} T_r(\mathbf{x}) E(X_1/R) \frac{x_2^2}{R^2} e^{i\pi/4} e^{ikR} \quad (54)$$

By almost identical arguments the reflected wave field is given by

$$u_3^2(\mathbf{x}) = \frac{ka}{\pi} \left(\frac{2\pi}{kR} \right)^{1/2} E(X_1/R) \frac{|x_2|}{R} e^{i\pi/4} [e^{-ikR} - iR_e(\mathbf{x})e^{ikR}] \quad (55)$$

where the pointwise reflection coefficient $R_e(\mathbf{x})$ is

$$R_e(\mathbf{x}) = \frac{ih}{4E(X_1/R)|x_2|/R} \times \int_{-1}^1 e^{ik\phi(X_1, x_2; s-av)} \left(\frac{R(X_1, x_2)}{R(X_1 + s - av, x_2)} \right)^{1/2} \left[\frac{\hat{\sigma}_{31}(av)}{\mu} \sin \theta - \frac{\hat{\sigma}_{32}(av)}{\mu} \cos \theta - i \frac{\hat{p}_3(av)}{\rho c} \right] dv \quad (56)$$

Note that $R_e(\mathbf{x})$, while not identical to $T_r(\mathbf{x})$, has a similar structure. Again $\partial R_e / \partial x_2$ may be discarded in the calculation of τ_{32}^2 .

We are now in a position to evaluate both sides of Eq.(45). Using Eqs.(46), (47), (54) and (55) in the left hand side and noting that the polarizations on the right are given in terms of their Fourier coefficients by Eqs.(21a, b), it is readily shown that

$$\frac{i4\mu ka}{\pi}(Q-P) = -i\mu 2h \sum_{n=-N}^N E^*(n\pi/ka) e^{ik(n\pi/ka)s} (\xi_n + \kappa_n \xi_{2n}) \quad (57)$$

where

$$Q = \int_{-\theta_b}^{\theta_b} T_r(\theta) \cos^2 \theta E^*(\sin \theta) E(\sin \theta) d\theta \quad (58)$$

$$P = \int_{-\theta_b}^{\theta_b} \cos^2 \theta E^*(\sin \theta) E(\sin \theta) d\theta \quad (59)$$

$T_r(\theta) = T_r(\mathbf{x})|_{x_2=f}$ and $\tan \theta_b = 1/F$. The superscript * denotes the complex conjugate. In calculating P we have, just as in Eq.(51), neglected a term of $O(kd_a)^{-1}$ arising from the reflected part of the total wave field at S_e , where d_a is again the distance from an end point $\pm a$. The term Q represents the sum over the aperture S_r of all the scattered signals collected by it, while P is proportional to the time averaged power incident to the interface. We are therefore lead to define the *generalized transmission coefficient* \mathbf{T} as

$$\mathbf{T} = Q/P \quad (60)$$

To calculate a corresponding *generalized reflection coefficient* measured at S_e we repeat the preceding argument with u_3^1 set equal to Eq.(32), but with $E(n\pi/ka)$ replaced by its complex conjugate. We are lead to define the generalized reflection coefficient \mathbf{R} as

$$\mathbf{R} = \frac{1}{P} \int_{-\theta_b}^{\theta_b} R_e(\mathbf{x}) \cos^2 \theta E^*(\sin \theta) E(\sin \theta) d\theta \quad (61)$$

Further, it is readily shown that

$$\mathbf{R} = 1 - \mathbf{T} \quad (62)$$

even though this relation does not hold for the pointwise coefficients T_r and R_e . Finally, rearranging Eq.(57) we obtain expressions for both generalized transmission and reflection coefficients in terms of the Fourier coefficients of the interfacial polarizations, namely,

$$\mathbf{R} = 1 - \mathbf{T} = \frac{h\pi}{2kaP} \sum_{n=-N}^N E^*(n\pi/ka) e^{in\pi s/a} (\xi_n + \kappa_n \xi_{2n}) \quad (63)$$

If the system were perfectly focusing, then E would be constant and N infinite so that \mathbf{T} or \mathbf{R} would be entirely attributable to the object at $(s,0)$. That neither is the case means that the information detected by the finite apertures is necessarily limited. The number of Fourier coefficients recovered is limited and each is weighted by an E . Also, recall that the Fourier coefficients depend on the E , because they represent the response of the interface to the incident beam so that the right hand side of Eq.(63) is not linear in E .

Lastly we specialize the interface to that of an infinite, uniformly thick cavity $|x_2| < h$ on whose surfaces the traction vanishes. This interface might model a fully open crack and thus sound cannot be transmitted across it. The parameters for this case are

$$\eta(x_2) = 1, \quad \mu^* = 0 \quad \text{and} \quad \rho^* = 0 \quad (64)$$

from which it is readily shown that the exact solution for the Fourier coefficients of the polarizations is given by

$$h\xi_n = \frac{2E(n\pi/ka)}{\kappa_n} e^{-i(sn\pi/a + kh\kappa_n)} \left\{ \left(\frac{n\pi}{ka} \right)^2 [1 - \cos(kh\kappa_n)] + \sin(kh\kappa_n) \right\} \quad (65)$$

and

$$h\xi_{2n} = -2E(n\pi/ka) e^{-isn\pi/a} \sin(kh\kappa_n) (1 - e^{ikh\kappa_n})^{-1} \quad (66)$$

for $n \leq N$, with $\xi_n = 0$ and $\xi_{2n} = 0$ for $n > N$. Substituting these results into Eq.(63) and taking the limit as $h \rightarrow 0$ gives

$$\mathbf{R} = \frac{1}{P} \sum_{n=-N}^N (\pi\kappa_n/ka) E^*(n\pi/ka) E(n\pi/ka) \quad (67)$$

Finally we deduce that in the limit $ka \rightarrow \infty$ we obtain the expected result that $\mathbf{R} \rightarrow 1$. This argument serves two purposes. Firstly it underlines the asymptotic nature of the calculation. We require ka to be large and kh to be small, the assumptions with which we began. Secondly it provides support for our definition of the generalized reflection and transmission coefficients. Evidently \mathbf{T} and \mathbf{R} may be thought of as the measured responses at the receiving and emitting transducers, normalized relative to the reflection from a traction free surface. Apart from the anti-plane shear approximation, this is how Margetan et al³ define their reflection coefficient in their Eq.(6).

III NUMERICAL EXPERIMENTS

INSERT FIGURE 3

We describe two sets of numerical scattering experiments. In both $ka = 26.73$, a value corresponding to approximately 7.5 mm in water at 1 MHz. Further, we set $kh = 0.5$, a value consistent with our approximations. In each case the generalized reflection coefficient \mathbf{R} , Eq.(63), has been normalized by dividing it by the generalized reflection coefficient, Eq.(67), for a fully open crack. In all cases we plot the magnitude of \mathbf{R} . One horizontal unit in each numerically calculated figure is set to $ka/100$. Also we have taken care to select beam parameters that produce a focal region most of whose amplitude is concentrated in a region that is narrow with respect to the cell width $2a$. Figure 3 shows how this cross-section can be varied with b and F . The real part of u_3^i/U_3 is plotted. In the subsequent scattering calculations we have taken $b = 2$ and $F = 1$. This does give sidelobes that trail off into adjacent cells, but the main part of the beam stays within a cell and the sidelobes are weak.

INSERT TABLE I

To demonstrate the effects of varying the density and elastic moduli of the inclusions, we have considered a range of material contrasts M^* and D^* . In two instances the matrix is water which does not support shear waves. However, since the mathematical problem is identical to the scalar acoustic problem we are justified in estimating the appropriate contrasts using the compressional wave speeds. Thus if c_w is the speed of sound in water, then we have set $\mu_w = \rho_w c_w^2$. Table I shows the five sets of material

contrasts used in our calculations, as well as the materials used when estimating them. We picked combinations that would show the effects of a strong contrast in M^* or D^* singly or together. The case of yttria inclusions gives only a weak contrast and is plotted separately.

INSERT FIGURE 4

Our first set of numerical experiments is concerned with an array of identical circular cylindrical inclusions, the basic configuration being displayed in Fig. 4. Within each cell, the cylinders are equally spaced with the center to center distance set at $1/11$ of the total cell width. Each cylinder is h in radius and, using the previously selected values of kh and ka , $kh/ka = 0.0187$. The dotted cylinders are intended to indicate that, in some experiments, we remove individual members of the array to create symmetric or asymmetric arrangements of vacancies.

INSERT FIGURE 5

The calculation for the simplest situation where all the cylinders except the central one are removed is shown in Fig. 5. We note that both the magnitude and shape of the scan profile of the reflection coefficient is greatly affected by the contrasts, though it is appropriate to insert a cautionary word here. In the case of copper in water the proposed contrast M^* may well be beyond the range in which the solution could be regarded as accurate because the formal error term in the approximate representation, Eq.(18), of the scattered wave field is now multiplied by a large M^* .

INSERT FIGURES 6,7 and 8

The next example, Fig.6, is a symmetric array of seven cylinders placed in the cell so that there are vacancies at positions ± 1 , ± 2 and ± 5 , where we have numbered the array from left to right so that position 0 corresponds to the central cylinder. Observe that, for all four material contrasts, two large 'visible' holes appear, corresponding to the enhanced transmission at the vacancies. A similar and perhaps more dramatic demonstration is given in Fig.7 where the symmetry is destroyed by omitting the cylinders numbered 1 and 4. The last example, Fig.8, derived from our periodic cylindrical array is to superimpose the three previous scans for a single set of material contrasts. The numbers in the legend indicate the cylinders present (and not vacancies) in the array, the adjective symmetric implies that the same cylinders are present on the other side of the cell and the adjective

asymmetric that vacancies occur on one side only. In this case we take very small values of M^* and D^* , those for yttria in an IN100 matrix, to model a barely visible interface.

INSERT FIGURES 9 and 10

Our second experiment is principally concerned with objects that are essentially in direct contact with one another. We have taken a periodic interface consisting of two grazing sinusoidal profiles (Fig.9) where the only parameter we vary is the periodicity of the sine curve. Thus

$$\eta = h \cos(2M\pi x_1/a) \quad (68)$$

and M is the number of periods per half-cell width. The material contrasts used were those for copper inclusions in a water matrix. The final graph, Fig.10, shows that as this parameter is increased, the reflection tends to a constant function of the scan position. This is what we should expect once the incident beam insonifies a complete cycle of the interface.

IV CONCLUSIONS

The numerical experiments, whose results are displayed in Figs.5 to 8, demonstrate that the reflection coefficient represents an image of the interface, discriminating the geometry and contrast in material parameters, provided the scatterers are separated. The ratio of the center to center spacing to the diameter of the cylinders is $a/(11h) = 4.86$ so that the cylinders are well separated. Further, in Fig.10, we have illustrated that for closely spaced obstacles of a size comparable to that of the focal region there is essentially no resolution of the individual scatterers. This aspect is explored in greater detail in Yogewaren and Harris² in their Fig.8.

In this paper we have described a mathematical model of scattering from imperfect interfaces where two regions are separated by a thin heterogeneous layer of inclusions. The degree of flexibility in the latter is great. We are able to independently vary the geometry and constitution of the included imperfections provided that a characteristic thickness is less than the interrogating wavelength. The model is founded on three ideas. Firstly, the sources of the scatter may be accurately represented by the through-thickness mean stress and momentum polarizations. Secondly, the response of a coaxial confocal pair of transducers may be represented in terms of certain well defined generalized transmission and reflection coefficients. These coefficients take account of the fact that, while many signals are collected by its aperture, essentially the transducer acts reciprocally and responds most strongly to the signals that phase match with the emitted signal. The mathematical device of introducing a large scale periodic structure effectively truncates the ideally infinite domain of integration to a finite region, greatly facilitating the numerical calculations. There are limitations to the current approach that we expect to address in future articles. We have only calculated the anti-plane case. However, the analysis carries over in a straightforward manner to the in-plane and possibly the three-dimensional cases. Lastly, we have yet to make comparisons of our model with measurements. One motivation for this article is to stimulate the design of relevant experiments.

Acknowledgments

The work was supported by the National Science Foundation through grant no. MSS-9114547. The contribution of GRW was supported in part by the Applied Mathematical Sciences subprogram of the Office of Energy Research, USDOE, contract no. W-7405-ENG-82. We thank F. Margetan, DOE Ames Laboratory, for helpful discussions on the measurement aspects of the work.

References

- ¹ G.R. Wickham, J. Nondestr. Eval. **11**, 199-210 (1992).
- ² E.Yogeswaren and J.G.Harris, J. Acoust. Soc.**96**, to appear (1994).
- ³ F.J. Margetan, R.B. Thompson, J.H. Rose and T.A. Gray, J. Nondestr. Eval. **11**, 109-26 (1992).
- ⁴ A. Bostrom, in *Ultrasonic Characterization and Mechanics of Interfaces*, AMD-Vol. **177**, ed. S.I. Rokhlin, S.K. Datta and Y.D.S. Rajapakse (ASME, New York, 1993), pp.191-197.
- ⁵ C. Pecorari, D.A. Mendelsohn and L. Adler , in *Ultrasonic Characterization and Mechanics of Interfaces*, AMD-Vol. **177**, ed. S.I. Rokhlin, S.K. Datta and Y.D.S. Rajapakse (ASME, New York, 1993), pp.207-221.
- ⁶ J.Qu in *Ultrasonic Characterization and Mechanics of Interfaces*, AMD-Vol. **177**, ed. S.I. Rokhlin, S.K. Datta and Y.D.S. Rajapakse (ASME, New York, 1993), pp.223-238.
- ⁷ J.D. Achenbach, M. Kitahara, Y. Mikata and D.A. Sotiropoulos, Pure Appl. Geophys. **128**, 101-118 (1988).
- ⁸ K. Shiloh, L.J. Bond and A.K. Som, Ultrasonics **31**, 395-404 (1993)

⁹ R.G. Thompson, C.J. Fiedler and O. Buck, in *Nondestructive Methods for Material Property Determination*, ed. C.O. Rund and R.E. Green (Plenum, New York, 1984), pp. 161-170.

¹⁰ I. Stakgold, *Boundary Value Problems of Mathematical Physics* (Macmillan, London, 1967), Vol.1, pp.44-47

¹¹ G.R. Wickham, Wave Motion, submitted (1994).

¹² D.A. Rebinsky and J.G. Harris, Proc. R. Soc. Lond. A **436**, 251-265 (1992).

¹⁴ E.T. Copson, *Asymptotic Expansions*, (University Press, Cambridge, 1971), pp.21-26.

Table I for An integrated model of scattering from an imperfect interface by
J.G. Harris, D.A. Rebinsky and G.R. Wickham

Table I

Materials	M^*	D^*
Gold inclusions in glass	-0.014	6.70
Glass inclusions in water	12.0	1.50
Copper inclusions in water	85.0	7.90
Gold inclusions in lucite	19.0	15.0
Yttria inclusions in IN100	-0.230	-0.360

A list of the material contrasts used for the numerical experiments. Recall that $D^* = (\rho^*/\rho - 1)$ and $M^* = (\mu^*/\mu - 1)$.

Figure captions for **An integrated model of scattering from an imperfect interface** by J.G. Harris, D.A. Rebinsky and G.R. Wickham

Figure 1 The geometrical configuration of a typical interface to be interrogated.

Figure 2 The geometry of the focused beam scanning the interface.

Figure 3 Cross-sections, at the focal plane, of the real part of u_3^i/U_3 . One horizontal unit equals $ka/100$.

Figure 4 A model interface comprised of an array of 11 cylinders equally spaced. The dashed cylinders may be imagined as removed from the array.

Figure 5 The magnitude of the generalized reflection coefficient for a single cylinder symmetrically placed within the cell for the first 4 material contrasts listed in Table I. One horizontal unit equals $ka/100$.

Figure 6 The magnitude of the reflection from a symmetric array for the first 4 material contrasts listed in Table I. Vacancies at positions ± 1 , ± 2 and ± 5 . One horizontal unit equals $ka/100$.

Figure 7 The magnitude of the reflection from an asymmetric array for the first 3 material contrasts listed in Table I. Vacancies at 1 and 4. One horizontal unit equals $ka/100$.

Figure 8 The magnitude of the reflection from three different arrays of yttria cylinders embedded in IN100. One horizontal unit equals $ka/100$.

Figure 9 A model interface consisting of grazing sinusoids.

Figure 10 The magnitude of the reflection from the interface comprised of grazing sinusoids for copper inclusions in a water matrix. One horizontal unit equals $ka/100$.

Fig.1 Harris, Rebinsky and Wickham

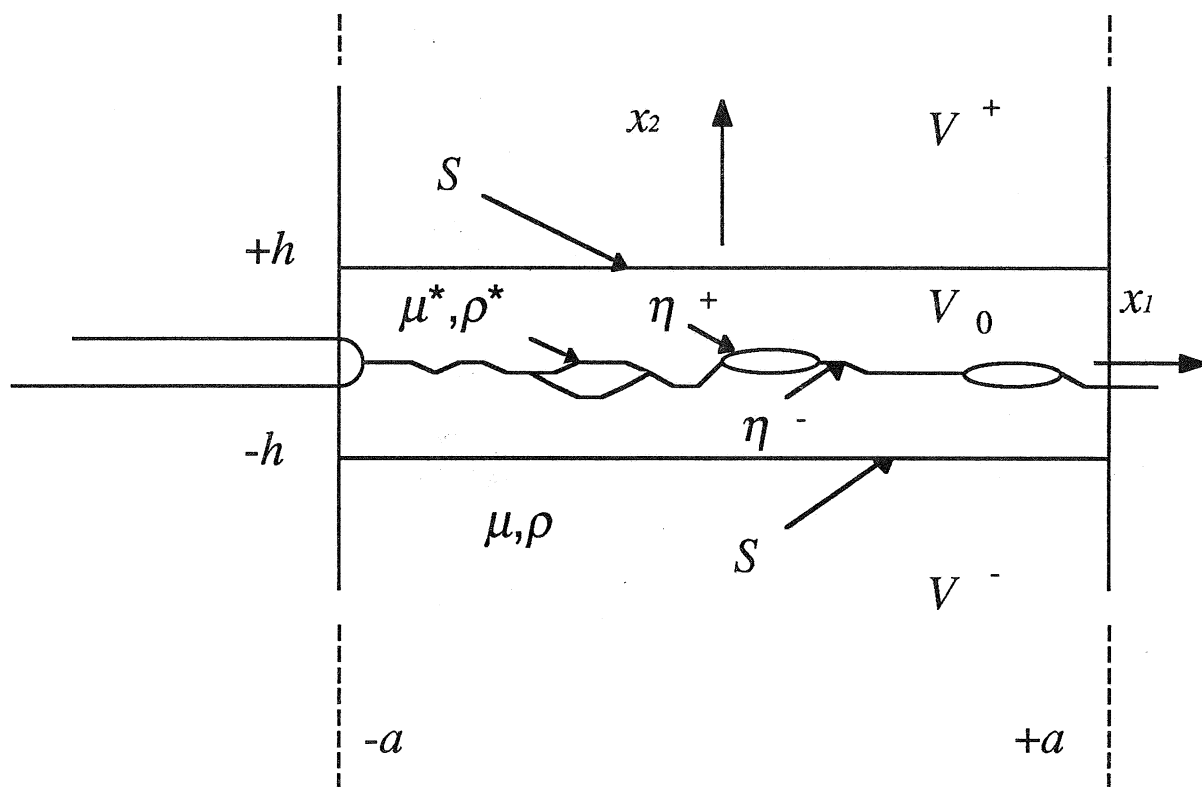


Fig.2 Harris, Rebinsky and Wickham

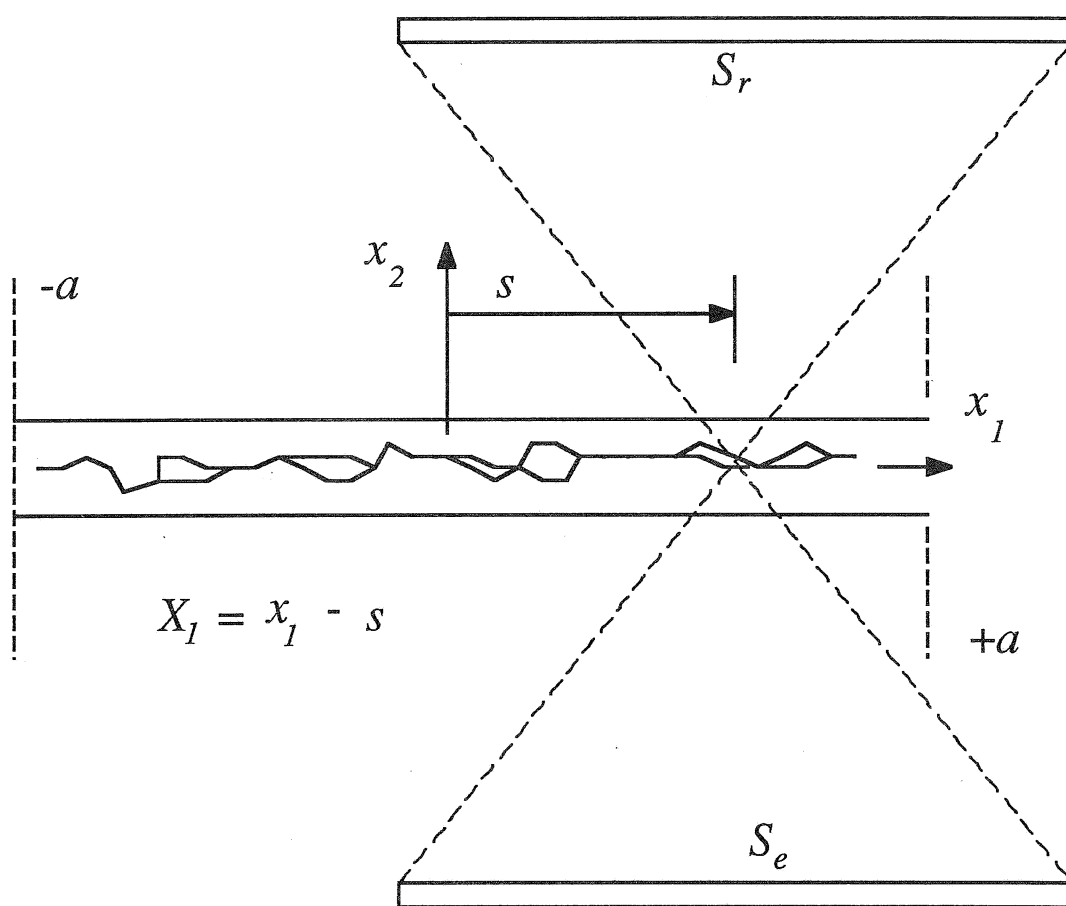


Fig.3 Harris, Rebinsky and Wickham

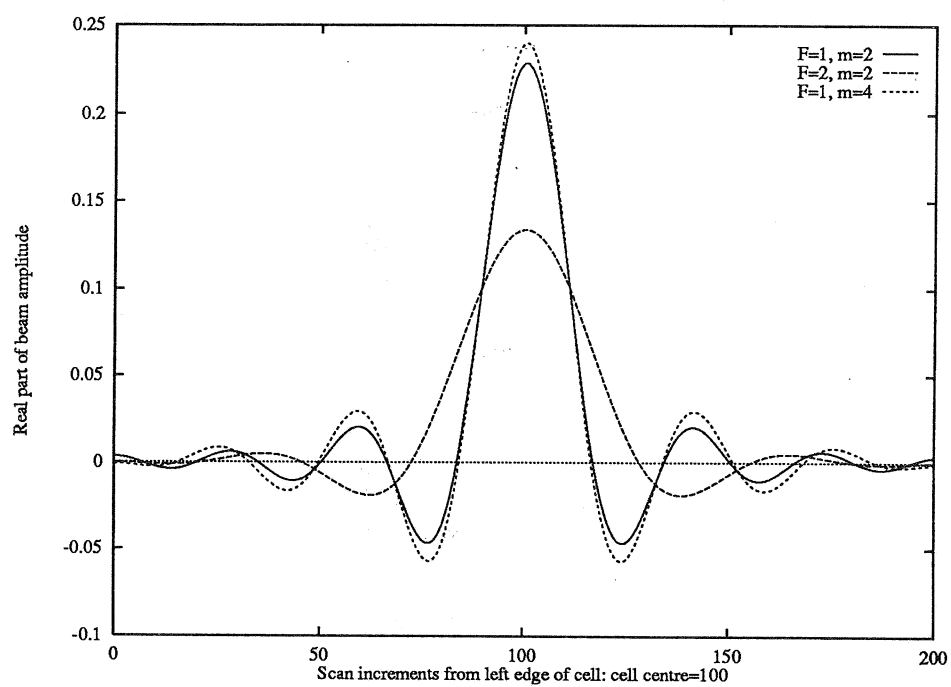


Fig.4 Harris, Rebinsky and Wickham

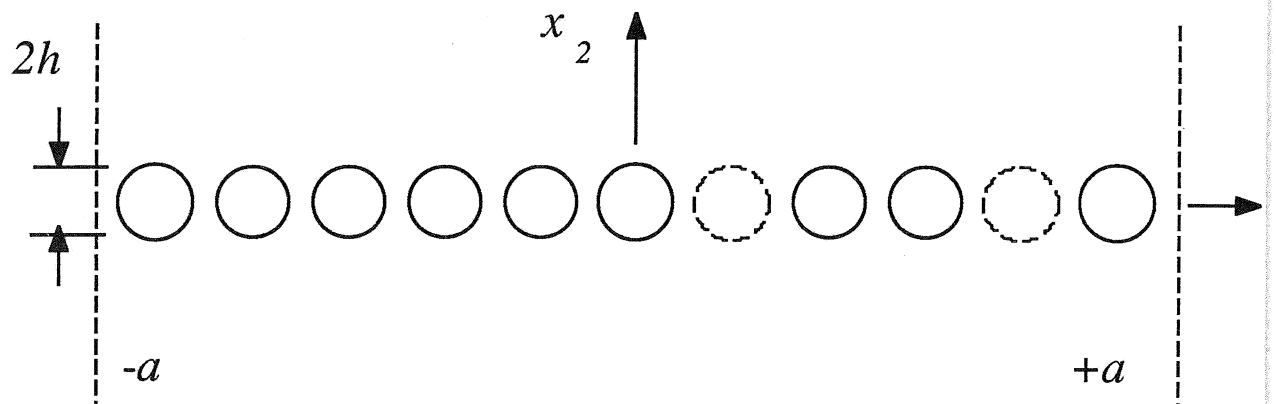


Fig.5 Harris, Rebinsky and Wickham

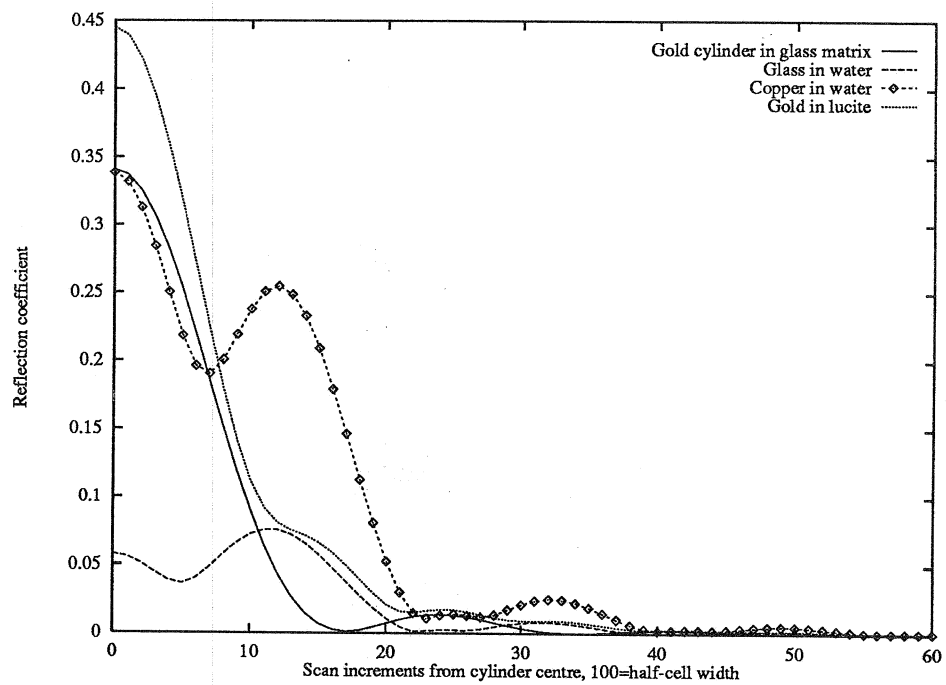


Fig.6 Harris, Rebinsky and Wickham

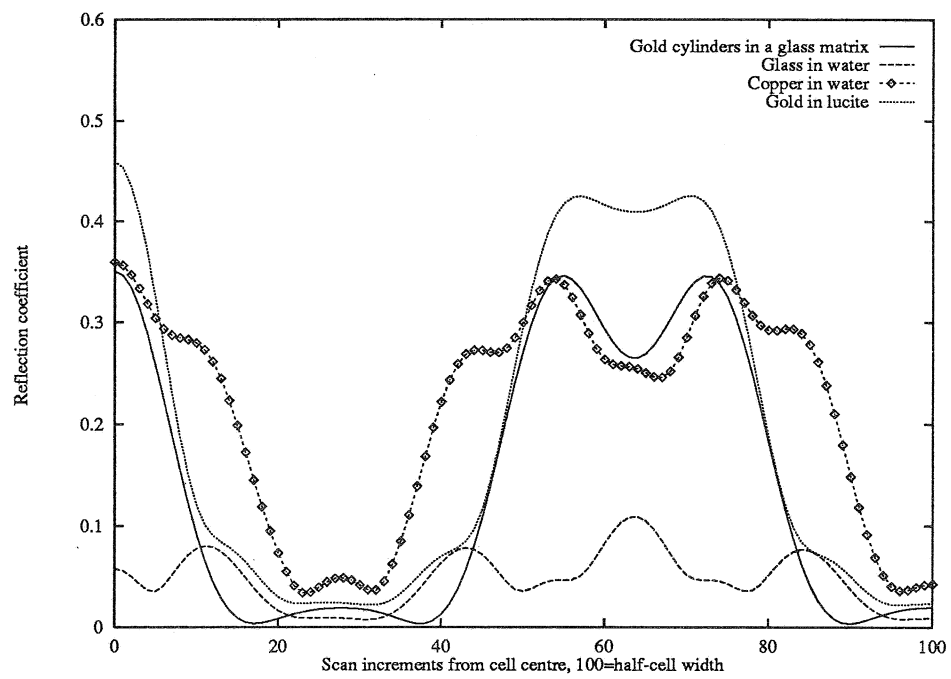


Fig.7 Harris, Rebinsky and Wickham

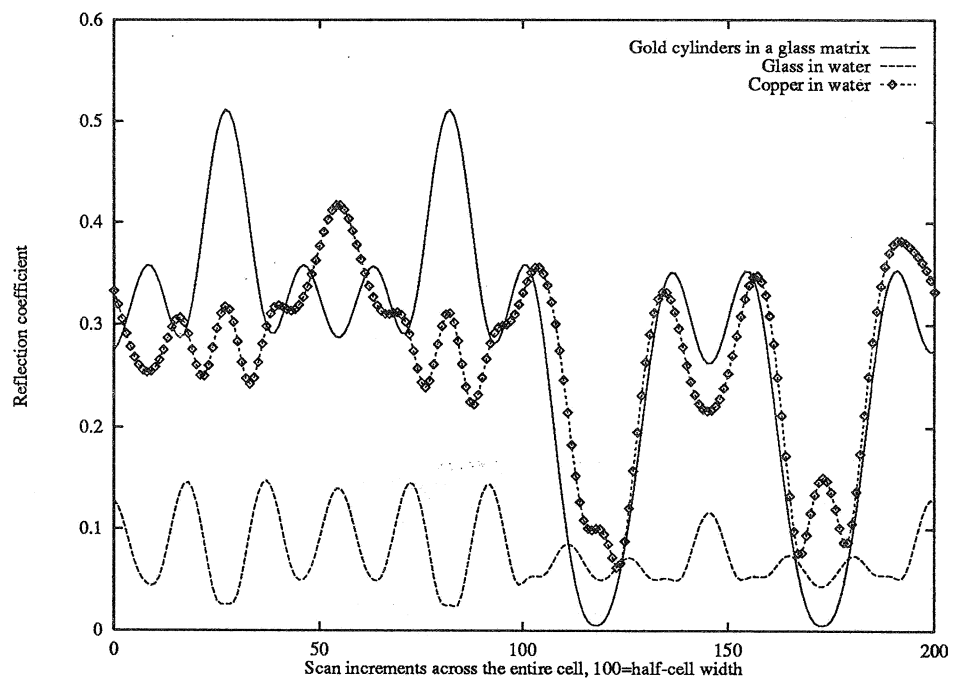


Fig.8 Harris, Rebinsky and Wickham

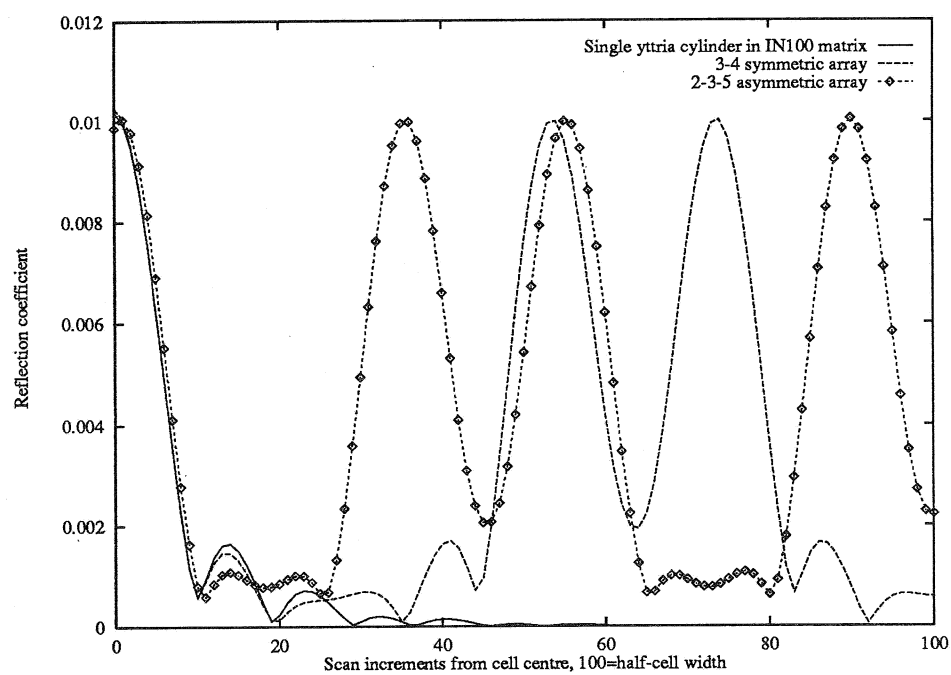


Fig.9 Harris, Rebinsky and Wickham

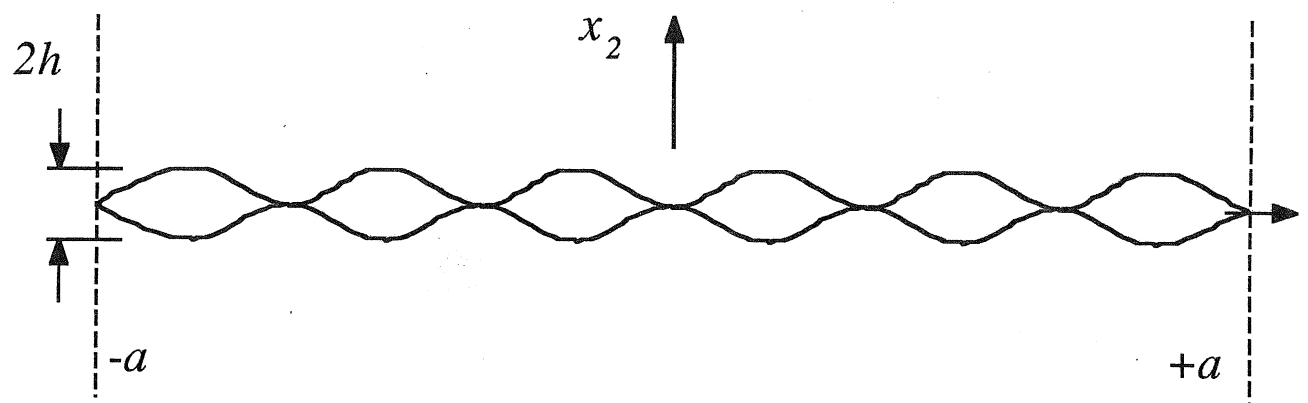
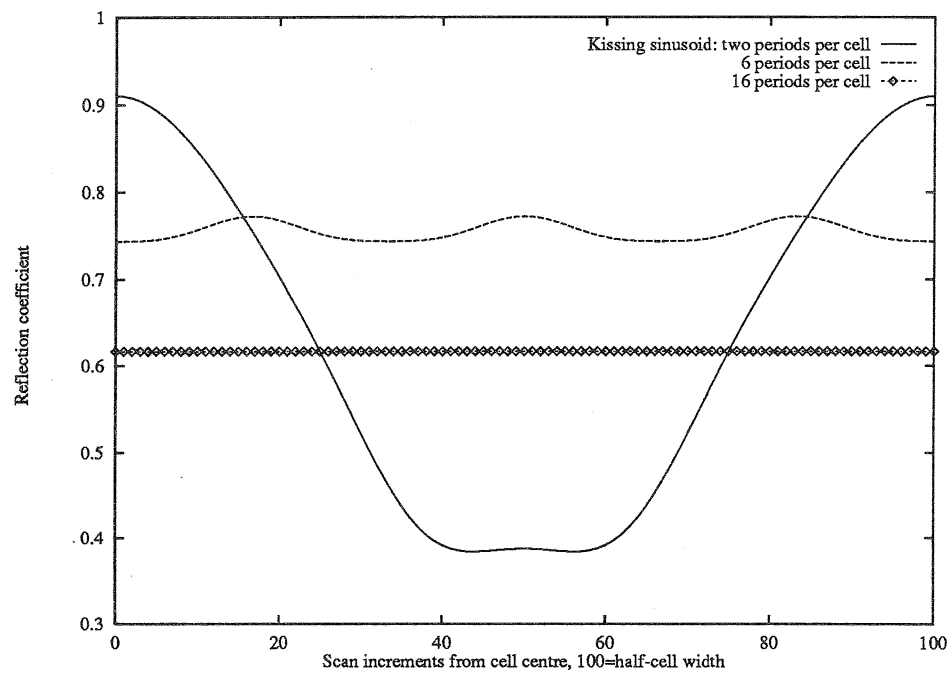


Fig.10 Harris, Rebinsky and Wickham



List of Recent TAM Reports

No.	Authors	Title	Date
717	Nitzsche, V. R., and K. J. Hsia	Modelling of dislocation mobility controlled brittle-to-ductile transition	July 1993
718	Hsia, K. J., and A. S. Argon	Experimental study of the mechanisms of brittle-to-ductile transition of cleavage fracture in silicon single crystals	July 1993
719	Cherukuri, H. P., and T. G. Shawki	An energy-based localization theory: Part II—Effects of the diffusion, inertia and dissipation numbers	Aug. 1993
720	Aref, H., and S. W. Jones	Chaotic motion of a solid through ideal fluid	Aug. 1993
721	Stewart, D. S.	Lectures on detonation physics: Introduction to the theory of detonation shock dynamics	Aug. 1993
722	Lawrence, C. J., and R. Mei	Long-time behavior of the drag on a body in impulsive motion	Sept. 1993
723	Mei, R., J. F. Klausner, and C. J. Lawrence	A note on the history force on a spherical bubble at finite Reynolds number	Sept. 1993
724	Qi, Q., R. E. Johnson, and J. G. Harris	A re-examination of the boundary layer attenuation and acoustic streaming accompanying plane wave propagation in a circular tube	Sept. 1993
725	Turner, J. A., and R. L. Weaver	Radiative transfer of ultrasound	Sept. 1993
726	Yogeswaren, E. K., and J. G. Harris	A model of a confocal ultrasonic inspection system for interfaces	Sept. 1993
727	Yao, J., and D. S. Stewart	On the normal detonation shock velocity-curvature relationship for materials with large activation energy	Sept. 1993
728	Qi, Q.	Attenuated leaky Rayleigh waves	Oct. 1993
729	Sofronis, P., and H. K. Birnbaum	Mechanics of hydrogen-dislocation-impurity interactions: Part I—Increasing shear modulus	Oct. 1993
730	Hsia, K. J., Z. Suo, and W. Yang	Cleavage due to dislocation confinement in layered materials	Oct. 1993
731	Acharya, A., and T. G. Shawki	A second-deformation-gradient theory of plasticity	Oct. 1993
732	Michaleris, P., D. A. Tortorelli, and C. A. Vidal	Tangent operators and design sensitivity formulations for transient nonlinear coupled problems with applications to elasto-plasticity	Nov. 1993
733	Michaleris, P., D. A. Tortorelli, and C. A. Vidal	Analysis and optimization of weakly coupled thermo-elasto-plastic systems with applications to weldment design	Nov. 1993
734	Ford, D. K., and D. S. Stewart	Probabilistic modeling of propellant beds exposed to strong stimulus	Nov. 1993
735	Mei, R., R. J. Adrian, and T. J. Hanratty	Particle dispersion in isotropic turbulence under the influence of non-Stokesian drag and gravitational settling	Nov. 1993
736	Dey, N., D. F. Socie, and K. J. Hsia	Static and cyclic fatigue failure at high temperature in ceramics containing grain boundary viscous phase: Part I—Experiments	Nov. 1993
737	Dey, N., D. F. Socie, and K. J. Hsia	Static and cyclic fatigue failure at high temperature in ceramics containing grain boundary viscous phase: Part II—Modelling	Nov. 1993
738	Turner, J. A., and R. L. Weaver	Radiative transfer and multiple scattering of diffuse ultrasound in polycrystalline media	Nov. 1993
739	Qi, Q., and R. E. Johnson	Resin flows through a porous fiber collection in pultrusion processing	Dec. 1993
740	Weaver, R. L., W. Sachse, and K. Y. Kim	Transient elastic waves in a transversely isotropic plate	Dec. 1993
741	Zhang, Y., and R. L. Weaver	Scattering from a thin random fluid layer	Dec. 1993
742	Weaver, R. L., and W. Sachse	Diffusion of ultrasound in a glass bead slurry	Dec. 1993

(continued on next page)

List of Recent TAM Reports (cont'd)

<i>No.</i>	<i>Authors</i>	<i>Title</i>	<i>Date</i>
743	Sundermeyer, J. N., and R. L. Weaver	On crack identification and characterization in a beam by nonlinear vibration analysis	Dec. 1993
744	Li, L., and N. R. Sottos	Predictions of static displacements in 1-3 piezocomposites	Dec. 1993
745	Jones, S. W.	Chaotic advection and dispersion	Jan. 1994
746	Stewart, D. S., and J. Yao	Critical detonation shock curvature and failure dynamics: Developments in the theory of detonation shock dynamics	Feb. 1994
747	Mei, R., and R. J. Adrian	Effect of Reynolds-number-dependent turbulence structure on the dispersion of fluid and particles	Feb. 1994
748	Liu, Z.-C., R. J. Adrian, and T. J. Hanratty	Reynolds-number similarity of orthogonal decomposition of the outer layer of turbulent wall flow	Feb. 1994
749	Barnhart, D. H., R. J. Adrian, and G. C. Papen	Phase-conjugate holographic system for high-resolution particle image velocimetry	Feb. 1994
750	Qi, Q., W. D. O'Brien Jr., and J. G. Harris	The propagation of ultrasonic waves through a bubbly liquid into tissue: A linear analysis	Mar. 1994
751	Mittal, R., and S. Balachandar	Direct numerical simulation of flow past elliptic cylinders	May 1994
752	Anderson, D. N., J. R. Dahlen, M. J. Danyluk, A. M. Dreyer, K. M. Durkin, J. J. Kriegsmann, J. T. McGonigle, and V. Tyagi	Thirty-first student symposium on engineering mechanics, J. W. Phillips, coord.	May 1994
753	Thoroddsen, S. T.	The failure of the Kolmogorov refined similarity hypothesis in fluid turbulence	May 1994
754	Turner, J. A., and R. L. Weaver	Time dependence of multiply scattered diffuse ultrasound in polycrystalline media	June 1994
755	Riahi, D. N.	Finite-amplitude thermal convection with spatially modulated boundary temperatures	June 1994
756	Riahi, D. N.	Renormalization group analysis for stratified turbulence	June 1994
757	Riahi, D. N.	Wave-packet convection in a porous layer with boundary imperfections	June 1994
758	Jog, C. S., and R. B. Haber	Stability of finite element models for distributed-parameter optimization and topology design	July 1994
759	Qi, Q., and G. J. Brereton	Mechanisms of removal of micron-sized particles by high-frequency ultrasonic waves	July 1994
760	Shawki, T. G.	On shear flow localization with traction-controlled boundaries	July 1994
761	Balachandar, S., D. A. Yuen, and D. M. Reuteler	High Rayleigh number convection at infinite Prandtl number with temperature-dependent viscosity	July 1994
762	Phillips, J. W.	Arthur Newell Talbot—Proceedings of a conference to honor TAM's first department head and his family	Aug. 1994
763	Man., C. S., and D. E. Carlson	On the traction problem of dead loading in linear elasticity with initial stress	Aug. 1994
764	Zhang, Y., and R. L. Weaver	Leaky Rayleigh wave scattering from elastic media with random microstructures	Aug. 1994
765	Cortese, T. A., and S. Balachandar	High-performance spectral simulation of turbulent flows in massively parallel machines with distributed memory	Aug. 1994
766	Balachandar, S.	Signature of the transition zone in the tomographic results extracted through the eigenfunctions of the two-point correlation	Sept. 1994
767	Piomelli, U.	Large-eddy simulation of turbulent flows	Sept. 1994
768	Harris, J. G., D. A. Rebinsky, and G. R. Wickham	An integrated model of scattering from an imperfect interface	Sept. 1994